



Article

WS_(1-x)Se_x Nanoparticles Decorated Three-Dimensional Graphene on Nickel Foam: A Robust and Highly Efficient Electrocatalyst for the Hydrogen Evolution Reaction

Sajjad Hussain^{1,2}, Kamran Akbar^{3,4}, Dhanasekaran Vikraman⁵ , Rana Arslan Afzal², Wooseok Song⁶, Ki-Seok An⁶ , Ayesha Farooq⁷, Jun-Young Park², Seung-Hyun Chun³ and Jongwan Jung^{1,2,*}

¹ Graphene Research Institute, Sejong University, Seoul 05006, Korea; hussain@sejong.ac.kr

² Institute of Nano and Advanced Materials Engineering, Sejong University, Seoul 05006, Korea; raafzal@hotmail.com (R.A.A.); jyoung@sejong.ac.kr (J.-Y.P.)

³ Department of Physics, Sejong University, Seoul 05006, Korea; mohkamranakbar@gmail.com (K.A.); schun@sejong.ac.kr (S.-H.C.)

⁴ Department of Energy Science, Sungkyunkwan University, Suwon 16419, Korea

⁵ Division of Electronics and Electrical Engineering, Dongguk University-Seoul, Seoul 04620, Korea; v.j.dhanasekaran@gmail.com

⁶ Thin Film Materials Research Center, Korea Research Institute of Chemical Technology, Daejeon 34114, Korea; wssong@kriect.re.kr (W.S.); ksan@kriect.re.kr (K.-S.A.)

⁷ Department of Physics, COMSATS IIT, Islamabad 45550, Pakistan; ayscha_farooq@comsats.edu.pk

* Correspondence: jwjung@sejong.ac.kr; Tel.: +82-2-3408-3688

Received: 5 October 2018; Accepted: 4 November 2018; Published: 8 November 2018



Abstract: To find an effective alternative to scarce, high-cost noble platinum (Pt) electrocatalyst for hydrogen evolution reaction (HER), researchers are pursuing inexpensive and highly efficient materials as an electrocatalyst for large scale practical application. Layered transition metal dichalcogenides (TMDCs) are promising candidates for durable HER catalysts due to their cost-effective, highly active edges and Earth-abundant elements to replace Pt electrocatalysts. Herein, we design an active, stable earth-abundant TMDCs based catalyst, WS_(1-x)Se_x nanoparticles-decorated onto a 3D porous graphene/Ni foam. The WS_(1-x)Se_x/graphene/NF catalyst exhibits fast hydrogen evolution kinetics with a moderate overpotential of ~ -93 mV to drive a current density of 10 mA cm⁻², a small Tafel slope of ~ 51 mV dec⁻¹, and a long cycling lifespan more than 20 h in 0.5 M sulfuric acid, which is much better than WS₂/NF and WS₂/graphene/NF catalysts. Our outcomes enabled a way to utilize the TMDCs decorated graphene and precious-metal-free electrocatalyst as mechanically robust and electrically conductive catalyst materials.

Keywords: hydrogen evolution reaction; electrocatalysts; electrocatalytic activity; TMDC

1. Introduction

Water splitting is widely considered to be an effective route for renewable, clean, and efficient energy production from the abundant water on Earth. Electrocatalytic or photocatalytic water splitting into oxygen and hydrogen may potentially address the global environmental pollution and energy crisis [1,2]. Platinum (Pt) has proved to be a most efficient hydrogen evolution reaction (HER) catalyst, however, it has low appeal to use in industrial applications due to its high cost and scarcity [3]. The development of an inexpensive, Earth-abundant, highly active, and acid-stable material to use as an electrocatalyst is a grand challenge. In recent years, tremendous effort has

been made to develop efficient HER catalysts from Earth-abundant materials with lots of active edges to replace Pt, such as transition-metal-based oxides/hydroxides, non-oxides, including metal based sulfides [4–6], selenides [7–9], carbides [10,11], phosphides [12,13], borate [14], phosphate [15], and their alloys. However, so far most of the catalysts exhibit inferior efficiency compared to Pt, while many processes involve complicated material synthesis and multiple steps, which may result in the increase of cost and further limit potential applications. Graphene is a well-known material, and it has potential for use in various electrocatalyst applications, which include supercapacitor, HER, and DSSCs [16,17]. Recently, tungsten disulfide (WS_2), which is from the family of transition metal dichalcogenides (TMDCs), has been studied elaborately as an electrocatalyst due to its high electrocatalytic properties [18]. Various studies have been done to promote the electrocatalytic activity of WS_2 with the combination of highly conductive materials, such as macro- and meso-porous carbon materials, gold (Au), and carbon paper in a hybrid nature for oxygen and hydrogen evolution reactions (OER and HER). Davodi and co-workers [19,20] reported the nitrogen doped multi-walled carbon nanotube (MWCNT) and $Ni@γ-Fe_2O_3$ /MWCNTs functionalized with nitrogen-rich emeraldine salt for alkaline HER and OER processes. Luo et al. also demonstrated $Fe_3O_4@NiFe_xO_y$ core-shell nano-heterostructures toward the OER with an overpotential $-410\text{ mV}@1\text{ mA cm}^{-2}$ and Tafel slope of 48 mV dec^{-1} [21]. Zhou et al. [22] used 3D hybrids of WS_2 /graphene/Ni foam as a catalyst in HER application and observed the low overpotential of $-119\text{ mV}@10\text{ mA cm}^{-2}$, the small Tafel slope of $\sim 43\text{ mV dec}^{-1}$, and the large cathodic current density. Recently, Zhou et al. has reported ternary tungsten sulfoselenide ($WS_{2(1-x)}Se_{2x}$) particles with a 3D porous metallic $NiSe_2$ foam to have excellent catalytic performance with $-88\text{ mV}@10\text{ mA cm}^{-2}$ of overpotential, 46.7 mV dec^{-1} of Tafel slope, and $214.7\text{ }\mu\text{A cm}^{-2}$ of exchange current density [23]. Our group has recently demonstrated a facile way to prepare a MoS_2 QDs film using a solution process and WS_2 /CoSe₂ heterostructure for HER applications [24,25]. Moreover, ternary alloys of $MoS_{2(1-x)}Se_{2x}$ and $WS_{2(1-x)}Se_{2x}$ were synthesized as an electrocatalyst for HER by a sputtering-CVD process with the overpotentials of -141 and -167 mV to drive 10 mA cm^{-2} and Tafel slopes of 67 and 107 mV dec^{-1} , respectively [26].

Recently, many efficient strategies to increase the number of active edge sites with large surface areas, high porosity, and better intrinsic electrical conductivity or the contact between the catalyst and the electrode were adopted to increase the electrocatalytic activity of electrode material. Herein, we utilized a 3D porous structure nickel (Ni) foam (NF) as a highly conductive skeleton, and produced WS_2 /NF, WS_2 -decorated graphene/NF, and $WS_{(1-x)}Se_x$ nanoparticles-decorated graphene/NF catalysts for HER applications. The obtained electrodes exhibited low overpotentials of -145 , -115 , and -93 mV vs. RHE for WS_2 /NF, WS_2 /Graphene/NF, and $WS_{(1-x)}Se_x$ /graphene/NF, respectively, at 10 mA cm^{-2} . The small Tafel slope was obtained for $WS_{(1-x)}Se_x$ /graphene/NF (51 mV dec^{-1}) as compared to the WS_2 /NF and WS_2 /graphene/NF (62 and 63 mV dec^{-1} , respectively).

2. Experimental Details

2.1. Synthesis of Graphene/NF, WS_2 /Graphene/NF, and $WS_{(1-x)}Se_x$ /Graphene/NF

Initially, the Ni foam (NF) was cleaned with ultrasonic baths of acetone, ethanol, and deionized water, baked at $120\text{ }^\circ\text{C}$ for 5 min, and then annealed with a hydrogen (H_2)/argon (Ar) (30/50 sccm) environment at $900\text{ }^\circ\text{C}$ for 30 min in a quartz tube furnace to clean the surface of the Ni foam without breaking the vacuum. Then to prepare the graphene on NF, the mixture of H_2 /Ar/methane (CH_4) flow (H_2 /Ar/ CH_4 = 50:100:50 sccm) was maintained for 30 min. Subsequently, the H_2 / CH_4 flow gas channel was shut off, and then rapidly cooled to room temperature in Ar environment. Furthermore, prepared graphene/NF was used as substrate for the growth of WS_2 and $WS_{(1-x)}Se_x$.

For WS_2 growth, ammonium tetrathiotungstate ($(NH_4)_2WS_4$) (Sigma Aldrich, 99.97%) was used as the main source material. First, a precursor of $(NH_4)_2WS_4$ (0.2 g) was dissolved in *N,N*-Dimethylformamide (DMF) (20 mL), and then the solution was sonicated for 30 min. The 3D graphene/Ni foam was immersed into the prepared $(NH_4)_2WS_4$ solution and then baked at $100\text{ }^\circ\text{C}$

for 30 min. Finally, synthesized films were placed in an annealing chamber and heated up to 450 °C for 30 and 45 min in a sulfur or sulfur/selenium environment to form WS₂/Graphene/NF and WS_(1-x)Se_x/Graphene/NF. The gas flow Ar/H₂ flux (50/50 sccm) was maintained, and the pressure of chamber was kept at 2 × 10⁻² Torr. The same quantity of sulfur/selenium (0.3/0.3 g) powder was used.

2.2. Electrochemical Measurements

The electrochemical measurements were conducted in a three-electrode setup with a Biologic SP-300 workstation. The polarization curves were collected using a linear sweep voltammetry (LSV) with a scan rate of 10 mV.s⁻¹ in 0.5 M H₂SO₄ electrolyte at room temperature. For the LSV measurement, a saturated calomel reference electrode (SCE) was used as the reference electrode. WS₂(30 min)/NF, WS₂(45 min)/NF, WS₂/graphene/NF, and WS_(1-x)Se_x/graphene/NF were used as the working electrode. Also, a graphite rod was used as the counter electrode. All LSV measurements were probed in terms of SCE and then converted to an reversible hydrogen electrode (RHE) scale with the help of the following equation: E(RHE) = E(SCE) + E°(SCE) + 0.059 pH. Electrochemical impedance spectroscopy (EIS) measurements were carried out in a potentiostatic mode with a frequency range from 0.01 Hz to 100 kHz under an amplitude of 10 mV. All the LSV polarizations were recorded after the ohmic drop iR correction. The stability measurement was examined using a chronoamperometric analysis.

3. Results and Discussion

Initially, the graphene was grown on a 3D NF using a chemical vapor deposition (CVD), as reported previously [27]. WS₂ was further grown by a hydrothermal process using an (NH₄)₂WS₄ precursor on 3D graphene with NF. To improve the crystalline quality, the film was further annealed at 500 °C in a sulfur environment at 30~45 min to form WS₂ nanoparticle-decorated graphene on NF (WS₂/graphene/NF). To form WS_(1-x)Se_x nanoparticles-decorated graphene on NF (WS_(1-x)Se_x/graphene/NF), a CVD deposited film was annealed at 450 °C in a sulfur and selenium environment at 30 min, respectively, to form WS_(1-x)Se_x onto graphene. The schematic representation is given in Figure 1.



Figure 1. Schematic preparation process of graphene and the WS_(1-x)Se_x/graphene/NF catalyst.

The surface morphological analysis was performed using a field emission scanning electron microscopy (FESEM) and a high-resolution transmission electron microscopy (HRTEM). Figure 2a–d shows the typical FESEM images of graphene, WS₂/NF, WS₂/graphene/NF, and WS_(1-x)Se_x/graphene/NF, respectively, and its insets show the higher magnification images. The bare NF (Figure 2a) is composed of lots of pores with sizes in tens to hundreds of micrometers, which will lead to somewhat irregular and uneven film growth which will be beneficial to enhance the HER property. From the FESEM image (Figure 2b), the regular deposition of graphene onto NF is observed with different thicknesses on the curvature of the foam. The larger area FESEM images of WS₂/NF, WS₂/graphene/NF, and WS_(1-x)Se_x/graphene/NF are provided in Figure S1. Wrinkles and ripples of graphene are spotted, which might be contributed to the differences in thermal expansion coefficients between the graphene and the Ni substrate [28]. The direct synthesis of WS₂ on NF,

for comparison, showed agglomerated small spherical granules with a non-uniform shape on the surface of the NF due to their curvature nature (Figure 2c). The nanoparticles with different sizes, due to agglomeration, were observed for WS₂/graphene/NF from the low and higher magnification FESEM images (Figure 2d). In the case of WS_(1-x)Se_x/graphene/NF, the stacked nano-plate like agglomerated grains were observed as shown in Figure 2e. The elemental composition of WS_(1-x)Se_x alloys were determined by the energy dispersion spectra (EDS) as presented in Figure S2 (WS_(1-x)Se_x —W: 32.0%, S: 16.3%, C: 4.8%, and Se: 8.0%). Ni signals are ascribed from the NF substrate. The elemental mapping images of WS₂ and WS_(1-x)Se_x layers are provided in Figures S3 and S4, and it confirms the homogeneous spatial distribution of W, S, C, and Se on the whole surface. The HRTEM studies were performed to reveal the layer structure of the prepared films. From the HRTEM images (Figure 3a), the multilayer of graphene was identified. In Figure 3b, WS_(1-x)Se_x and graphene are shown with yellow and red boxes, respectively.

Figures 2 and 3 suggest the expose of active edge sites at the surface of WS_(1-x)Se_x/graphene/NF particles as reported in previous literature [23,29]. The WS_(1-x)Se_x nanosheets, with an interlayer separation of 0.64 nm, were grown intimately on the graphene/NF substrate, which are also beneficial to enhance a HER reaction.

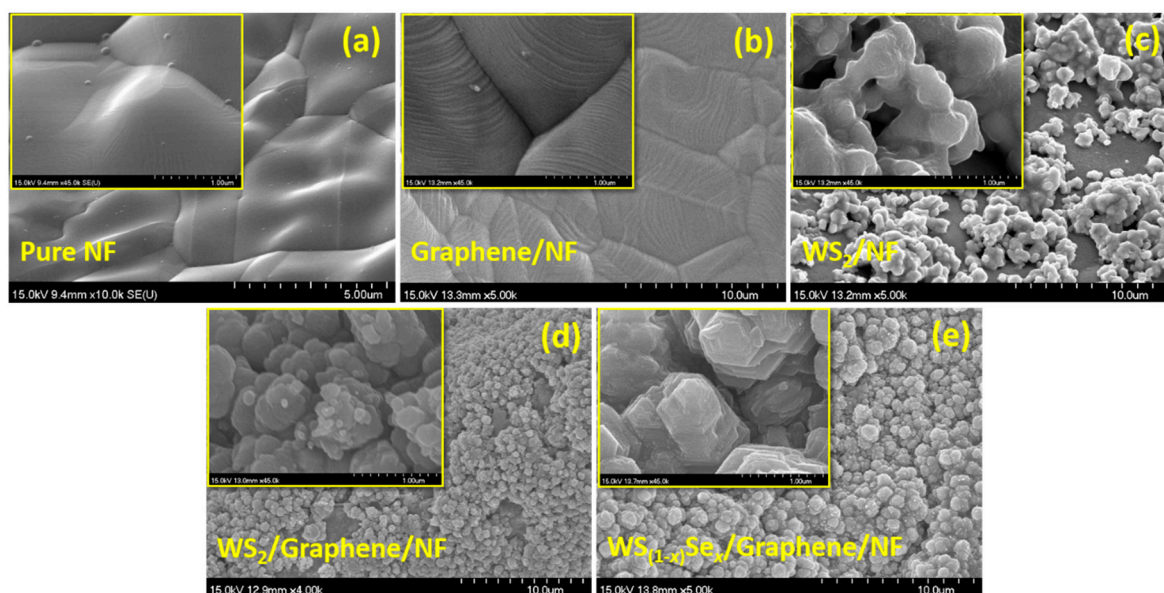


Figure 2. SEM micrographs of (a) pure NF; (b) graphene/NF; (c) WS₂(45 min)/NF; (d) WS₂/graphene/NF and (e) WS_(1-x)Se_x/graphene/NF.

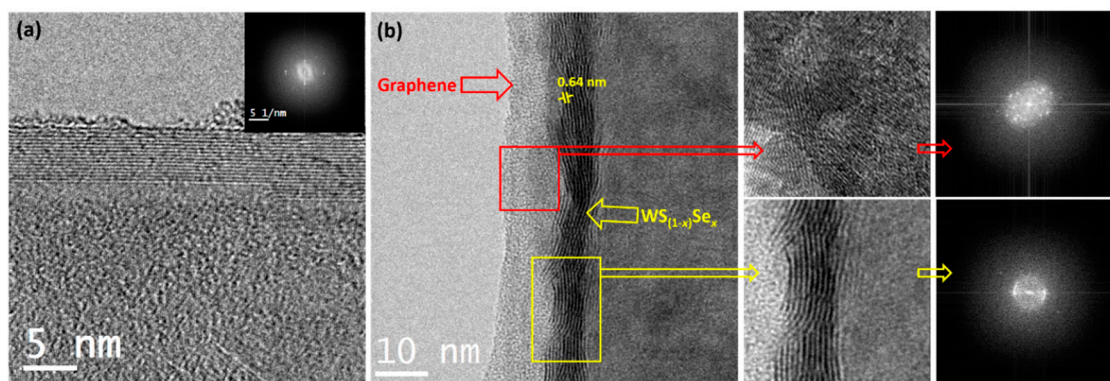


Figure 3. HRTEM images of (a) graphene/NF and (b) WS_(1-x)Se_x/graphene/NF. The layer spacing value is indicated as 0.64 nm, which is related to a (002) lattice plane d-spacing value. High-resolution HRTEM images show the corresponding graphene (red line) and WS_(1-x)Se_x (yellow line) lattice structures with selected area electron diffraction (SAED) pattern.

Raman spectroscopy was further used to characterize the formation of graphene, WS₂/NF, WS₂/graphene/NF, and WS_(1-x)Se_x/graphene/NF. From the spectrum of graphene/NF (Figure 4a), the principle bands of graphene, such as G band (1577 cm⁻¹), 2D band (2706 cm⁻¹), and D band (1364 cm⁻¹) were exhibited due to defects in the carbon lattice [30]. For WS₂/NF, two prominent Raman peaks originated at 350.1 and 420.5 cm⁻¹ correspond to the E¹_{2g} and A_{1g} modes, respectively [31]. In the case of WS₂/graphene/NF, E¹_{2g} and A_{1g} modes (351.6 and 420.5 cm⁻¹) for WS₂, two sharp peaks for graphene (G band: 1577.8 cm⁻¹ and 2D band: 2699.8 cm⁻¹) are shown [32,33]. In addition to the above peaks, a low intensity E¹_{2g} mode peak was observed at 250.6 cm⁻¹, corresponding to WSe₂ [34] for WS_(1-x)Se_x/graphene/NF. Our results also confirm the formation of both WS₂ and WSe₂ on porous graphene foam. Furthermore, the observed Raman results are well consistent with previously reported results of a WS₂ and WSe₂ materials system [34].

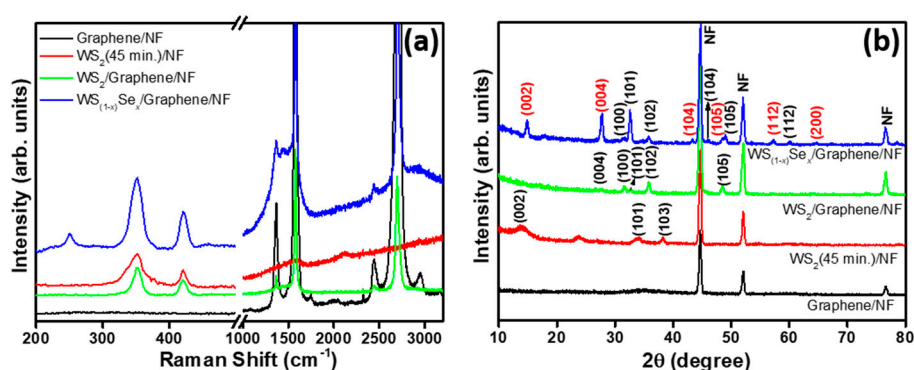


Figure 4. (a) Raman and (b) XRD spectra of graphene/NF, WS₂(45 min)/NF, WS₂/graphene/NF and WS_(1-x)Se_x/graphene/NF.

The structural and chemical composition of the graphene, WS₂/NF, WS₂/3D graphene, and WS_(1-x)Se_x/graphene/NF were further investigated via an X-ray diffraction (XRD) and X-ray photoelectron (XPS), respectively. The XRD patterns of graphene, WS₂/NF, WS₂/3D graphene, and WS_(1-x)Se_x/graphene/NF samples are shown in Figure 4b. No distinguishable diffraction signals were observed from graphene/NF due to their relatively low diffraction intensity. For WS₂/NF (Figure 4b), the peaks appeared at 14.1°, 33.1°, and 38.3° that correspond to the (002), (101), and (103) lattice planes, respectively, which are consistent with hexagonally structured WS₂ (WS₂: JCPDS 657515). For WS₂/graphene/NF, (004), (100), (101), (102), and (105) peaks were observed for WS₂. In the case of WS_(1-x)Se_x/graphene/NF, WSe₂ (002), (004), (104), (105), (112), and (200) lattice planes appeared in addition to the WS₂/graphene/NF peaks as shown in Figure 3b (WSe₂: JCPDS No. 89-5257). From the XPS survey scan of WS₂/graphene/NF (Figure S5), the observation of C, Ni, W, and S elements was confirmed. For WS_(1-x)Se_x/graphene/NF (Figure 5a), an additional peak of Se element was detected. The expanded region of W4f, S2p, C, and Se3d peaks are provided in the Figure 5b–e. A sharp peak at 284 eV originated from graphene. The two principal peaks of W binding energy of 4f_{7/2} and W 4f_{5/2} (36.4 and 34.5 eV) doublets, which were indicative of the oxidation state of W⁴⁺, appeared. The S 2p_{1/2} and 2p_{3/2} orbital peaks observed at 163.6 and 161.9 eV, respectively, indicating the S₂, confirmed the WS₂ crystal [31,35]. The Se 3d core levels can be fitted with Se 3d_{5/2} (53.8 eV) and Se 3d_{3/2} (55.6 eV) corresponding to the −2 oxidation state of selenium [36].

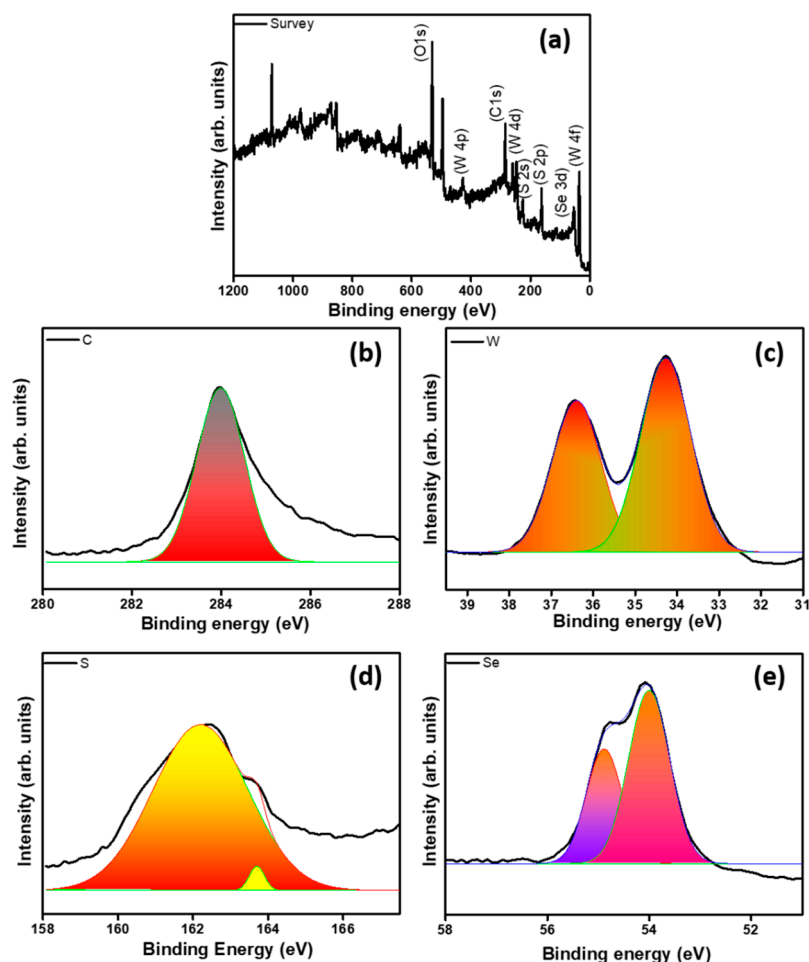


Figure 5. X-ray photoemission spectroscopy scan for $WS_{(1-x)}Se_x$ /graphene/NF. (a) Survey scan; (b) C, (c) W; (d) S and (e) Se binding energies.

HER activities were investigated via a standard three-electrode setup with a scan rate of 10 mV s^{-1} in 0.5 M sulfuric acid (H_2SO_4) electrolyte solution by linear sweep voltammetry (LSV) with iR correction. As expected, the commercial Pt wire exhibited the lowest overpotential, which was close to zero. The $WS_{(1-x)}Se_x$ /graphene/NF catalyst can deliver an overpotential at -93 mV vs. the reversible hydrogen electrode (RHE) for a geometric current density of 10 mA cm^{-2} . In contrast, $WS_2(45 \text{ min})/\text{NF}$, and $WS_2/\text{graphene}/\text{NF}$ exhibited inferior HER activity (-114 and -115 mV vs. RHE at current 10 mA cm^{-2} , respectively) (Figure 6a,b). Earlier research reported that the unsaturated Se facets are highly active and improve HER activity [37,38]. Theoretical estimation supports lower Gibbs free energy for H_2 adsorption onto the Se facets than the S facets [38]. Graphene is a conductive material which can increase the conduction between electrode and electrolyte and create the synergistic effect with active materials that lead to good HER properties.

The catalytic overpotential (-93 mV) of the $WS_{(1-x)}Se_x$ /graphene/NF was quite lower than those of the reported WS_2 -based TMDs in the literature, which include: Cobalt sulfide @ WS_2 /carbon cloth (CC) hybrid catalyst ($-97.2 \text{ mV}@10 \text{ mA cm}^{-2}$) [39], WS_2 /reduced graphene oxide hybrid nanosheets ($-150 \sim -200 \text{ mV}@10 \text{ mA cm}^{-2}$) [40], MoS_2 - WS_2 ($-129 \text{ mV}@10 \text{ mA cm}^{-2}$) [41], WS_2 @hollow nitrogen-doped carbon nanofibers ($-185 \text{ mV}@10 \text{ mA cm}^{-2}$) [42], graphdiyne- WS_2 2D-nanohybrid electrocatalysts ($-140 \text{ mV}@10 \text{ mA cm}^{-2}$) [43], and $\text{Mo}_{(1-x)}W_xS_2$ hollow nanospheres on an Ni_3S_2 nanorod ($-98 \text{ mV}@10 \text{ mA cm}^{-2}$) [44]. For comparison, graphene on NF and WS_2 (annealed at 30 min in an S environment) on NF were used as electrocatalysts, and their LSV curves are provided in the supporting information Figure S6 (overpotential of -193 and -145 mV vs. RHE, respectively).

The inherent property of catalytic activity for HER kinetics was probed by extracting the slopes from the linear regions in Tafel plots. A Tafel slope of 51 mV dec^{-1} was extracted for $\text{WS}_{(1-x)}\text{Se}_x/\text{graphene}/\text{NF}$, which is close to the value of a commercial Pt catalyst, and 62 mV and 63 mV dec^{-1} were obtained for $\text{WS}_2(45 \text{ min})/\text{graphene}/\text{NF}$ and WS_2/NF , respectively (Figure 6c). The Tafel slope, 51 mV dec^{-1} of $\text{WS}_{(1-x)}\text{Se}_x/\text{graphene}/\text{NF}$, was lower than those of the previously reported WS_2 -based catalysts as well as other hybrid catalysts for HER, such as 3D $\text{WS}_2/\text{graphene}/\text{Ni}$ (87 mV dec^{-1}) [45], nanostructured WS_2/CC ($127\sim 105 \text{ mV dec}^{-1}$) [46], bulk WS_2 and WS_2 nanosheets on bare oxidized carbon fiber (OCF) ($149 \sim 99 \text{ mV dec}^{-1}$) [47], $\text{WS}_2 @\text{WS}_2$ nanorattles, WS_2 nanoflakes and bulk WS_2 ($68, 71$ and 92 mV dec^{-1}) [48], vertically-oriented WS_2 nanosheet/graphene (73 mV dec^{-1}) [49], WSe_2 and $\text{WS}_{2(1-x)}\text{Se}_{2x}$ nanotubes (105 and 99 mV dec^{-1}) [50], and monolayer of WS_2 and $\text{WS}_{2(1-x)}\text{Se}_{2x}$ with a tunable band gap (100 and 85 mV dec^{-1}) [51]. Previous research demonstrated the influence of Se inclusion to create the abundant active edges which can be promote HER properties and hence to perceive the low overpotential and small Tafel slope [52].

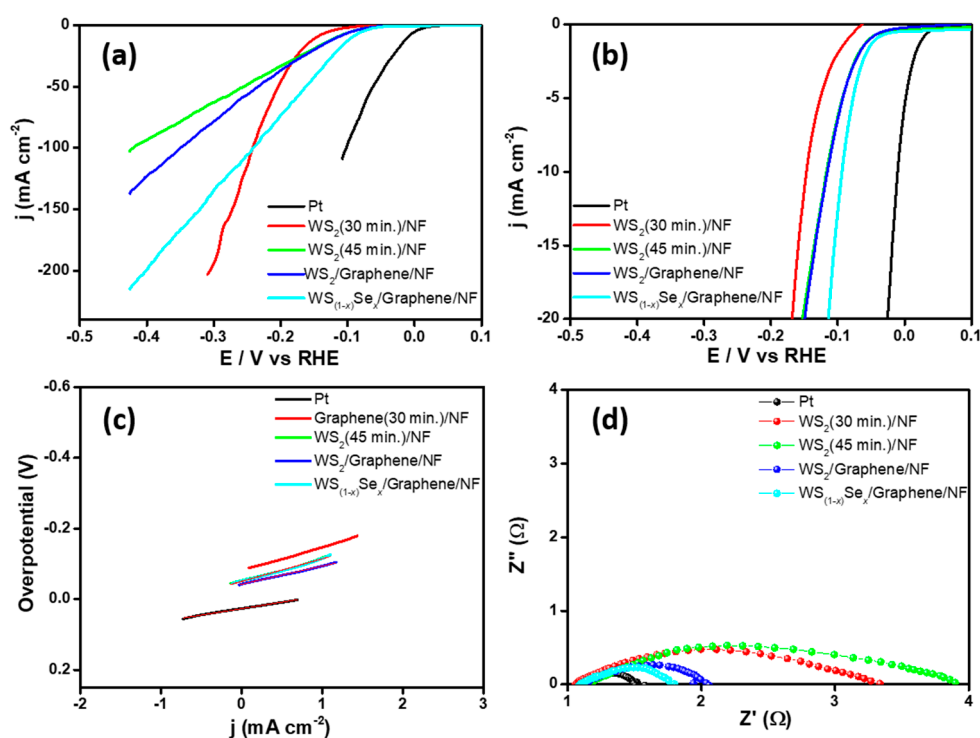


Figure 6. Electrochemical performance of different electrocatalysts. (a,b) Linear sweep voltammetry (LSV) curves of Pt, $\text{WS}_2(45 \text{ min})/\text{NF}$, $\text{WS}_2/\text{graphene}/\text{NF}$ and $\text{WS}_{(1-x)}\text{Se}_x/\text{graphene}/\text{NF}$ electrocatalyst with scan rate @ 10 mV s^{-1} ; (c) corresponding Tafel plots obtained from the LSV curves; (d) EIS spectra for Pt, $\text{WS}_2(45 \text{ min})/\text{NF}$, $\text{WS}_2/\text{graphene}/\text{NF}$ and $\text{WS}_{(1-x)}\text{Se}_x/\text{graphene}/\text{NF}$ electrocatalyst.

The exchange current density (j_0) was found to be ~ 0.162 , ~ 0.165 , and $\sim 0.274 \text{ mA cm}^{-2}$, for WS_2/NF , $\text{WS}_2/\text{graphene}/\text{NF}$ and $\text{WS}_{(1-x)}\text{Se}_x/\text{graphene}/\text{NF}$, respectively. The observed high j_0 for $\text{WS}_{(1-x)}\text{Se}_x/\text{graphene}/\text{NF}$ may be attributed to the large number of exposed active edge sites, good electrical conductivity, or the porous structure. The observed HER parameters for different electrodes are listed in Table 1. In acid solutions, three controlled reactions occur when hydrogen evolves on a metal chalcogenide catalyst. The overall HER reaction may proceed via a discharge step (Volmer-reaction, Equation (1)) followed by the ion-atom reaction (Heyrovsky reaction, Equation (2)) that leads to a Tafel slope of 40 mV dec^{-1} , or a combination reaction (Tafel-reaction, Equation (3)) that leads to a Tafel slope of 30 mV dec^{-1} .





From the classical theory for hydrogen evolution process, the observed Tafel slope of 36 mV dec^{-1} for Pt exposes the hydrogen production proceeds with the fast discharge step (Equation (1)) followed by the Tafel (Equation (3)) [53,54]. The observed intermediate Tafel slope values of 51, 62, and $63 \text{ mV} \cdot \text{dec}^{-1}$ (WS_2/NF , $\text{WS}_2/\text{graphene}/\text{NF}$ and $\text{WS}_{(1-x)}\text{Se}_x/\text{graphene}/\text{NF}$, respectively) suggest that hydrogen production proceeds with the fast discharge step (equation 1) followed by the Tafel (Equation (3)) or Heyrovsky ion-atom reaction (Equation (2)) [17,55,56]. The observed small overpotential and Tafel slope for $\text{WS}_{(1-x)}\text{Se}_x/\text{graphene}/\text{NF}$ could be attributed to the nanostructured particles on the porous substrate, which increase accessible active sites.

Table 1. Comparison of catalytic parameters of different HER catalysts.

Catalyst	Overpotential (mV vs. RHE) @10 mA cm ⁻²	Tafel Slope (mV dec ⁻¹)	Exchange Current Density (j ₀ , mA cm ⁻²)
Pt	−10	36	5.98
WS ₂ (45 min)/NF	−115	63	0.162
WS ₂ /graphene/NF	−114	62	0.165
WS _(1-x) Se _x /graphene/NF	−93	51	0.274

EIS was performed to study the interface reactions and electrode kinetics in HER at a frequency range from 0.01 Hz to 100 kHz. The Nyquist plots revealed the charge-transfer resistance (R_{ct}) of Pt, $\text{WS}_2(45 \text{ min})/\text{NF}$, $\text{WS}_2/\text{graphene}/\text{NF}$, and $\text{WS}_{(1-x)}\text{Se}_x/\text{graphene}/\text{NF}$. The R_{ct} value of Pt, $\text{WS}_2(45 \text{ min})/\text{NF}$, $\text{WS}_2/\text{graphene}/\text{NF}$, and $\text{WS}_{(1-x)}\text{Se}_x/\text{graphene}/\text{NF}$ were approximately 0.5, 2.4, 1.1, and 0.8Ω , respectively (Figure 6d). The lower R_{ct} value suggests a faster reaction rate between the electrode and electrolyte. The low R_{ct} value could be due to the abundance of accessible sulfur/salination active edges on a 3D porous substrate and result in the higher HER activity.

Stability is another key factor to elucidate the performance of catalysts. For this purpose, we tested the stability of $\text{WS}_{(1-x)}\text{Se}_x/\text{graphene}/\text{NF}$ electrode using potential cycling in the range from -0.5 to $+0.1 \text{ V}$ with a scan rate of $50 \text{ mV} \cdot \text{s}^{-1}$. After a 20 h operation in a $0.5 \text{ M H}_2\text{SO}_4$ solution, the polarization curve was little changed from the initial one, which indicated no observable degradation after long-term cycling tests (Figure 7a). The long-term electrochemical stability of this electrode was also examined. The cathodic current density for the $\text{WS}_{(1-x)}\text{Se}_x/\text{graphene}/\text{NF}$ catalyst remained stable and exhibited no obvious degradation for electrolysis at a fixed overpotential of -93 mV for more than 20 h, which indicated the potential usage of this catalyst maintained its catalytic activity over a long time in the electrochemical process (Figure 7b).

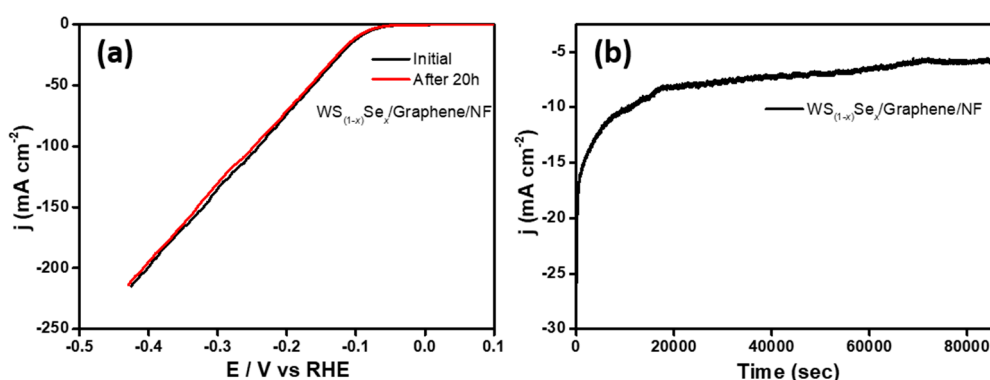


Figure 7. LSV curves for $\text{WS}_{(1-x)}\text{Se}_x/\text{graphene}/\text{NF}$ before and after 20 h HER performance. Time dependent current density variation of $\text{WS}_{(1-x)}\text{Se}_x/\text{graphene}/\text{NF}$ catalyst at a constant applied potential of -93 mV for more than 20 h.

4. Conclusions

In summary, an effective and efficient strategy was adopted for the synthesis of WS₂ and ternary WS_(1-x)Se_x/graphene/NF for a robust and stable self-standing hydrogen evolving catalyst. The novel WS_(1-x)Se_x/graphene/NF catalyst showed good HER catalytic properties in acidic electrolyte with an overpotential of −93 mV to drive 10 mA cm^{−2}, a small Tafel slope of 51 mV dec^{−1}, and a high exchange current density with excellent long-term durability. Our results proved that Se incorporated WS₂/graphene/NF exhibits the highest electrocatalytic activity for HER, and it is stable in acidic media over a long period among the other electrodes due to high active edge sites and porous structures.

Supplementary Materials: The following are available online at <http://www.mdpi.com/2079-4991/8/11/929/s1>, Figure S1: Low magnification of FESEM images. (a) WS₂(45 min)/NF; (b) WS₂/graphene/NF and (c) WS_(1-x)Se_x/graphene/NF. Figure S2: EDS spectrum for WS_(1-x)Se_x/graphene/NF. Figure S3: (a) FESEM image of WS₂/graphene/NF and its elemental mapping images of (b) Ni (c) W (d) S and (e) Se elements. Figure S4: (a) FESEM image of WS_(1-x)Se_x/graphene/NF and its elemental mapping images of (b) Ni (c) W (d) C (e) S and (f) Se elements. Figure S5: X-ray photoemission spectroscopy scan for WS₂(45 min)/graphene/NF. (a) survey scan; (b) C; (c) W; and (d) S binding energies. Figure S6: Linear sweep voltammetry curves of graphene/NF and WS₂(30 min.) /NF electrocatalyst.

Author Contributions: S.H. and K.A. initiated the study, performed the extensive experiments, and wrote the Manuscript with assistance from the co-authors. D.V. analyzed the data. A.F. and R.A.A. performed extensive experiment to measure electrochemical properties. W.S. and K.-S.A. performed XPS and analyses data. S.-H.C., J.-Y.P., and J.J. participation included planning, experimental work, and discussion. All authors read and approved the final manuscript.

Acknowledgments: This research was supported by the Basic Science Research Program through the National Research Foundation of Korea (NRF), funded by the Ministry of Education (2010-0020207, 2017R1C1B5076952), by the Nano Material Technology Development Program through the NRF funded by the Ministry of Science, ICT, and Future Planning (2016M3A7B4909942), and by the Korea Institute of Energy Technology Evaluation and Planning (KETEP) and the Ministry of Trade, Industry, and Energy (MOTIE) of the Republic of Korea (20172010106080).

Conflicts of Interest: The authors declare no conflicts of interest.

References

1. Xu, X.; Song, F.; Hu, X. A nickel iron diselenide-derived efficient oxygen-evolution catalyst. *Nat. Commun.* **2016**, *7*, 12324. [[CrossRef](#)] [[PubMed](#)]
2. Zhang, B.; Xiao, C.; Xie, S.; Liang, J.; Chen, X.; Tang, Y. Iron-Nickel Nitride Nanostructures in Situ Grown on Surface-Redox-Etching Nickel Foam: Efficient and Ultrasustainable Electrocatalysts for Overall Water Splitting. *Chem. Mater.* **2016**, *28*, 6934–6941. [[CrossRef](#)]
3. Reier, T.; Oezaslan, M.; Strasser, P. Electrocatalytic oxygen evolution reaction (OER) on Ru, Ir, and Pt catalysts: A comparative study of nanoparticles and bulk materials. *ACS Catal.* **2012**, *2*, 1765–1772. [[CrossRef](#)]
4. Zhang, B.; Zheng, X.; Voznyy, O.; Comin, R.; Bajdich, M.; García-Melchor, M.; Han, L.; Xu, J.; Liu, M.; Zheng, L. Homogeneously dispersed multimetal oxygen-evolving catalysts. *Science* **2016**, *352*, 333–337. [[CrossRef](#)] [[PubMed](#)]
5. Huang, J.; Chen, J.; Yao, T.; He, J.; Jiang, S.; Sun, Z.; Liu, Q.; Cheng, W.; Hu, F.; Jiang, Y. CoOOH nanosheets with high mass activity for water oxidation. *Angew. Chem. Int. Ed.* **2015**, *54*, 8722–8727. [[CrossRef](#)] [[PubMed](#)]
6. Singh, A.; Chang, S.L.; Hocking, R.K.; Bach, U.; Spiccia, L. Highly active nickel oxide water oxidation catalysts deposited from molecular complexes. *Energy Environ. Sci.* **2013**, *6*, 579–586. [[CrossRef](#)]
7. Xu, K.; Ding, H.; Jia, K.; Lu, X.; Chen, P.; Zhou, T.; Cheng, H.; Liu, S.; Wu, C.; Xie, Y. Solution-Liquid-Solid Synthesis of Hexagonal Nickel Selenide Nanowire Arrays with a Nonmetal Catalyst. *Angew. Chem. Int. Ed.* **2016**, *55*, 1710–1713. [[CrossRef](#)] [[PubMed](#)]
8. Wang, F.; Li, Y.; Shifa, T.A.; Liu, K.; Wang, F.; Wang, Z.; Xu, P.; Wang, Q.; He, J. Selenium-Enriched Nickel Selenide Nanosheets as a Robust Electrocatalyst for Hydrogen Generation. *Angew. Chem.* **2016**, *128*, 7033–7038. [[CrossRef](#)]
9. Vikraman, D.; Hussain, S.; Akbar, K.; Adakalam, K.; Lee, S.H.; Chun, S.-H.; Jung, J.; Kim, H.-S.; Park, H.J. Facile Synthesis of Molybdenum Diselenide Layers for High-Performance Hydrogen Evolution Electrocatalysts. *ACS Omega* **2018**, *3*, 5799–5807. [[CrossRef](#)]

10. Xu, K.; Ding, H.; Lv, H.; Chen, P.; Lu, X.; Cheng, H.; Zhou, T.; Liu, S.; Wu, X.; Wu, C. Dual Electrical-Behavior Regulation on Electrocatalysts Realizing Enhanced Electrochemical Water Oxidation. *Adv. Mater.* **2016**, *28*, 3326–3332. [[CrossRef](#)] [[PubMed](#)]
11. Wan, C.; Leonard, B.M. Iron-doped molybdenum carbide catalyst with high activity and stability for the hydrogen evolution reaction. *Chem. Mater.* **2015**, *27*, 4281–4288. [[CrossRef](#)]
12. Zhou, K.; Zhou, W.; Yang, L.; Lu, J.; Cheng, S.; Mai, W.; Tang, Z.; Li, L.; Chen, S. Ultrahigh-Performance Pseudocapacitor Electrodes Based on Transition Metal Phosphide Nanosheets Array via Phosphorization: A General and Effective Approach. *Adv. Funct. Mater.* **2015**, *25*, 7530–7538. [[CrossRef](#)]
13. Stern, L.-A.; Feng, L.; Song, F.; Hu, X. Ni₂P as a Janus catalyst for water splitting: The oxygen evolution activity of Ni₂P nanoparticles. *Energy Environ. Sci.* **2015**, *8*, 2347–2351. [[CrossRef](#)]
14. Chen, P.; Xu, K.; Zhou, T.; Tong, Y.; Wu, J.; Cheng, H.; Lu, X.; Ding, H.; Wu, C.; Xie, Y. Strong-Coupled Cobalt Borate Nanosheets/Graphene Hybrid as Electrocatalyst for Water Oxidation Under Both Alkaline and Neutral Conditions. *Angew. Chem. Int. Ed.* **2016**, *55*, 2488–2492. [[CrossRef](#)] [[PubMed](#)]
15. Ahn, H.S.; Tilley, T.D. Electrocatalytic water oxidation at neutral pH by a nanostructured Co(PO₃)₂ anode. *Adv. Funct. Mater.* **2013**, *23*, 227–233. [[CrossRef](#)]
16. Wang, X.; Zhi, L.; Müllen, K. Transparent, conductive graphene electrodes for dye-sensitized solar cells. *Nano Lett.* **2008**, *8*, 323–327. [[CrossRef](#)] [[PubMed](#)]
17. Li, Y.; Wang, H.; Xie, L.; Liang, Y.; Hong, G.; Dai, H. MoS₂ nanoparticles grown on graphene: An advanced catalyst for the hydrogen evolution reaction. *J. Am. Chem. Soc.* **2011**, *133*, 7296–7299. [[CrossRef](#)] [[PubMed](#)]
18. Cheng, L.; Huang, W.; Gong, Q.; Liu, C.; Liu, Z.; Li, Y.; Dai, H. Ultrathin WS₂ nanoflakes as a high-performance electrocatalyst for the hydrogen evolution reaction. *Angew. Chem. Int. Ed.* **2014**, *53*, 7860–7863. [[CrossRef](#)] [[PubMed](#)]
19. Davodi, F.; Mühlhausen, E.; Tavakkoli, M.; Sainio, J.; Jiang, H.; Gökce, B.; Marzun, G.; Kallio, T. Catalyst Support Effect on the Activity and Durability of Magnetic Nanoparticles: Toward Design of Advanced Electrocatalyst for Full Water Splitting. *ACS Appl. Mater. Interfaces* **2018**, *10*, 31300–31311. [[CrossRef](#)] [[PubMed](#)]
20. Davodi, F.; Tavakkoli, M.; Lahtinen, J.; Kallio, T. Straightforward synthesis of nitrogen-doped carbon nanotubes as highly active bifunctional electrocatalysts for full water splitting. *J. Catal.* **2017**, *353*, 19–27. [[CrossRef](#)]
21. Luo, Z.; Martí-Sánchez, S.; Nafria, R.; Joshua, G.; de la Mata, M.; Guardia, P.; Flox, C.; Martínez-Boubeta, C.; Simeonidis, K.; Llorca, J. Fe₃O₄@NiFe_xO_y Nanoparticles with Enhanced Electrocatalytic Properties for Oxygen Evolution in Carbonate Electrolyte. *ACS Appl. Mater. Interfaces* **2016**, *8*, 29461–29469. [[CrossRef](#)] [[PubMed](#)]
22. Zhou, H.; Yu, F.; Sun, J.; He, R.; Wang, Y.; Guo, C.F.; Wang, F.; Lan, Y.; Ren, Z.; Chen, S. Highly active and durable self-standing WS₂/graphene hybrid catalysts for the hydrogen evolution reaction. *J. Mater. Chem. A* **2016**, *4*, 9472–9476. [[CrossRef](#)]
23. Zhou, H.; Yu, F.; Sun, J.; Zhu, H.; Mishra, I.K.; Chen, S.; Ren, Z. Highly efficient hydrogen evolution from edge-oriented WS₂(1-x)Se_{2x} particles on three-dimensional porous NiSe₂ foam. *Nano Lett.* **2016**, *16*, 7604–7609. [[CrossRef](#)] [[PubMed](#)]
24. Vikraman, D.; Akbar, K.; Hussain, S.; Yoo, G.; Jang, J.-Y.; Chun, S.-H.; Jung, J.; Park, H.J. Direct synthesis of thickness-tunable MoS₂ quantum dot thin layers: Optical, structural and electrical properties and their application to hydrogen evolution. *Nano Energy* **2017**, *35*, 101–114. [[CrossRef](#)]
25. Hussain, S.; Akbar, K.; Vikraman, D.; Liu, H.; Chun, S.-H.; Jung, J. WS₂/CoSe₂ heterostructure: A designed structure as catalysts for enhanced hydrogen evolution performance. *J. Ind. Eng. Chem.* **2018**, *65*, 167–174. [[CrossRef](#)]
26. Hussain, S.; Akbar, K.; Vikraman, D.; Karuppasamy, K.; Kim, H.-S.; Chun, S.-H.; Jung, J. Synthesis of MoS₂(1-x)Se_{2x} and WS₂(1-x)Se_{2x} alloys for enhanced hydrogen evolution reaction performance. *Inorg. Chem. Front.* **2017**, *4*, 2068–2074. [[CrossRef](#)]
27. Hussain, S.; Akbar, K.; Vikraman, D.; Choi, D.-C.; Kim, S.J.; An, K.-S.; Jung, S.; Jung, J. A highly sensitive enzymeless glucose sensor based on 3D graphene-Cu hybrid electrodes. *New J. Chem.* **2015**, *39*, 7481–7487. [[CrossRef](#)]
28. Mattevi, C.; Kim, H.; Chhowalla, M. A review of chemical vapour deposition of graphene on copper. *J. Mater. Chem.* **2011**, *21*, 3324–3334. [[CrossRef](#)]

29. Jung, Y.; Shen, J.; Sun, Y.; Cha, J.J. Chemically synthesized heterostructures of two-dimensional molybdenum/tungsten-based dichalcogenides with vertically aligned layers. *ACS Nano* **2014**, *8*, 9550–9557. [[CrossRef](#)] [[PubMed](#)]
30. Gupta, A.; Chen, G.; Joshi, P.; Tadigadapa, S.; Eklund, P. Raman scattering from high-frequency phonons in supported n-graphene layer films. *Nano Lett.* **2006**, *6*, 2667–2673. [[CrossRef](#)] [[PubMed](#)]
31. Song, J.-G.; Park, J.; Lee, W.; Choi, T.; Jung, H.; Lee, C.W.; Hwang, S.-H.; Myoung, J.M.; Jung, J.-H.; Kim, S.-H.; et al. Layer-Controlled, Wafer-Scale, and Conformal Synthesis of Tungsten Disulfide Nanosheets Using Atomic Layer Deposition. *ACS Nano* **2013**, *7*, 11333–11340. [[CrossRef](#)] [[PubMed](#)]
32. Loh, T.A.; Chua, D.H.; Wee, A.T. One-step synthesis of few-layer WS₂ by pulsed laser deposition. *Sci. Rep.* **2015**, *5*, 18116. [[CrossRef](#)] [[PubMed](#)]
33. Sarma, P.V.; Patil, P.D.; Barman, P.K.; Kini, R.N.; Shaijumon, M.M. Controllable growth of few-layer spiral WS₂. *RSC Adv.* **2016**, *6*, 376–382. [[CrossRef](#)]
34. Li, S.; Wang, S.; Tang, D.-M.; Zhao, W.; Xu, H.; Chu, L.; Bando, Y.; Golberg, D.; Eda, G. Halide-assisted atmospheric pressure growth of large WSe₂ and WS₂ monolayer crystals. *Appl. Mater. Today* **2015**, *1*, 60–66. [[CrossRef](#)]
35. Ibrahim, M.A.; Lan, T.-W.; Huang, J.K.; Chen, Y.-Y.; Wei, K.-H.; Li, L.-J.; Chu, C.W. High quantity and quality few-layers transition metal disulfide nanosheets from wet-milling exfoliation. *RSC Adv.* **2013**, *3*, 13193–13202. [[CrossRef](#)]
36. Rhyee, J.S.; Kwon, J.; Dak, P.; Kim, J.H.; Kim, S.M.; Park, J.; Hong, Y.K.; Song, W.G.; Omkaram, I.; Alam, M.A. High-Mobility Transistors Based on Large-Area and Highly Crystalline CVD-Grown MoSe₂ Films on Insulating Substrates. *Adv. Mater.* **2016**, *28*, 2316–2321. [[CrossRef](#)] [[PubMed](#)]
37. Huang, Y.; Lu, H.; Gu, H.; Fu, J.; Mo, S.; Wei, C.; Miao, Y.-E.; Liu, T. A CNT@MoSe₂ hybrid catalyst for efficient and stable hydrogen evolution. *Nanoscale* **2015**, *7*, 18595–18602. [[CrossRef](#)] [[PubMed](#)]
38. Wang, H.; Kong, D.; Johanes, P.; Cha, J.J.; Zheng, G.; Yan, K.; Liu, N.; Cui, Y. MoSe₂ and WSe₂ nanofilms with vertically aligned molecular layers on curved and rough surfaces. *Nano Lett.* **2013**, *13*, 3426–3433. [[CrossRef](#)] [[PubMed](#)]
39. Zhou, X.; Yang, X.; Hedhili, M.N.; Huang, K.-W.; Li, L.-J.; Zhang, W. Symmetrical synergy of hybrid CoS₂-WS₂ electrocatalysts for hydrogen evolution reaction. *J. Mater. Chem. A* **2017**, *5*, 15552–15558. [[CrossRef](#)]
40. Yang, J.; Voiry, D.; Ahn, S.J.; Kang, D.; Kim, A.Y.; Chhowalla, M.; Shin, H.S. Two-Dimensional Hybrid Nanosheets of Tungsten Disulfide and Reduced Graphene Oxide as Catalysts for Enhanced Hydrogen Evolution. *Angew. Chem. Int. Ed.* **2013**, *52*, 13751–13754. [[CrossRef](#)] [[PubMed](#)]
41. Vikraman, D.; Hussain, S.; Akbar, K.; Truong, L.; Kathalingam, A.; Chun, S.-H.; Jung, J.; Park, H.J.; Kim, H.-S. Improved Hydrogen Evolution Reaction Performance using MoS₂-WS₂ Heterostructures by Physicochemical Process. *ACS Sustain. Chem. Eng.* **2018**, *6*, 8400–8409. [[CrossRef](#)]
42. Yu, S.; Kim, J.; Yoon, K.R.; Jung, J.-W.; Oh, J.; Kim, I.-D. Rational design of efficient electrocatalysts for hydrogen evolution reaction: Single layers of WS₂ nanoplates anchored to hollow nitrogen-doped carbon nanofibers. *ACS Appl. Mater. Interfaces* **2015**, *7*, 28116–28121. [[CrossRef](#)] [[PubMed](#)]
43. Yao, Y.; Jin, Z.; Chen, Y.; Gao, Z.; Yan, J.; Liu, H.; Wang, J.; Li, Y.; Liu, S.F. Graphdiyne-WS₂ 2D-Nanohybrid electrocatalysts for high-performance hydrogen evolution reaction. *Carbon* **2017**. [[CrossRef](#)]
44. Zheng, M.; Du, J.; Hou, B.; Xu, C.-L. Few-Layered Mo_(1-x)W_xS₂ Hollow Nanospheres on Ni₃S₂ Nanorod Heterostructure as Robust Electrocatalysts for Overall Water Splitting. *ACS Appl. Mater. Interfaces* **2017**, *9*, 26066–26076. [[CrossRef](#)] [[PubMed](#)]
45. Qi, F.; Li, P.; Chen, Y.; Zheng, B.; Liu, J.; Zhou, J.; He, J.; Hao, X.; Zhang, W. Three-dimensional structure of WS₂/graphene/Ni as a binder-free electrocatalytic electrode for highly effective and stable hydrogen evolution reaction. *Int. J. Hydrog. Energy* **2017**, *42*, 7811–7819. [[CrossRef](#)]
46. Yan, Y.; Xia, B.; Li, N.; Xu, Z.; Fisher, A.; Wang, X. Vertically oriented MoS₂ and WS₂ nanosheets directly grown on carbon cloth as efficient and stable 3-dimensional hydrogen-evolving cathodes. *J. Mater. Chem. A* **2015**, *3*, 131–135. [[CrossRef](#)]
47. Shang, X.; Yan, K.-L.; Liu, Z.-Z.; Lu, S.-S.; Dong, B.; Chi, J.-Q.; Li, X.; Liu, Y.-R.; Chai, Y.-M.; Liu, C.-G. Oxidized carbon fiber supported vertical WS₂ nanosheets arrays as efficient 3D nanostructure electrocatalysts for hydrogen evolution reaction. *Appl. Surf. Sci.* **2017**, *402*, 120–128. [[CrossRef](#)]
48. Wen, Y.; Xia, Y.; Zhang, S. Tungsten disulphide nanorattle: A new type of high performance electrocatalyst for hydrogen evolution reaction. *J. Power Sources* **2016**, *307*, 593–598. [[CrossRef](#)]

49. Shifa, T.A.; Wang, F.; Cheng, Z.; Zhan, X.; Wang, Z.; Liu, K.; Safdar, M.; Sun, L.; He, J. A vertical-oriented WS₂ nanosheet sensitized by graphene: An advanced electrocatalyst for hydrogen evolution reaction. *Nanoscale* **2015**, *7*, 14760–14765. [[CrossRef](#)] [[PubMed](#)]
50. Xu, K.; Wang, F.; Wang, Z.; Zhan, X.; Wang, Q.; Cheng, Z.; Safdar, M.; He, J. Component-Controllable WS_{2(1-x)}Se_{2x} Nanotubes for Efficient Hydrogen Evolution Reaction. *ACS Nano* **2014**, *8*, 8468–8476. [[CrossRef](#)] [[PubMed](#)]
51. Fu, Q.; Yang, L.; Wang, W.; Han, A.; Huang, J.; Du, P.; Fan, Z.; Zhang, J.; Xiang, B. Synthesis and enhanced electrochemical catalytic performance of monolayer WS_{2(1-x)}Se_{2x} with a tunable band gap. *Adv. Mater.* **2015**, *27*, 4732–4738. [[CrossRef](#)] [[PubMed](#)]
52. Gong, Q.; Cheng, L.; Liu, C.; Zhang, M.; Feng, Q.; Ye, H.; Zeng, M.; Xie, L.; Liu, Z.; Li, Y. Ultrathin MoS_{2(1-x)}Se_{2x} Alloy Nanoflakes For Electrocatalytic Hydrogen Evolution Reaction. *ACS Catal.* **2015**, *5*, 2213–2219. [[CrossRef](#)]
53. Thomas, J.G.N. Kinetics of electrolytic hydrogen evolution and the adsorption of hydrogen by metals. *Trans. Faraday Soc.* **1961**, *57*, 1603–1611. [[CrossRef](#)]
54. Merki, D.; Fierro, S.; Vrubel, H.; Hu, X. Amorphous molybdenum sulfide films as catalysts for electrochemical hydrogen production in water. *Chem. Sci.* **2011**, *2*, 1262–1267. [[CrossRef](#)]
55. Wang, F.; Li, J.; Wang, F.; Shifa, T.A.; Cheng, Z.; Wang, Z.; Xu, K.; Zhan, X.; Wang, Q.; Huang, Y. Enhanced Electrochemical H₂ Evolution by Few-Layered Metallic WS_{2(1-x)}Se_{2x} Nanoribbons. *Adv. Funct. Mater.* **2015**, *25*, 6077–6083. [[CrossRef](#)]
56. Xu, C.; Peng, S.; Tan, C.; Ang, H.; Tan, H.; Zhang, H.; Yan, Q. Ultrathin S-doped MoSe₂ nanosheets for efficient hydrogen evolution. *J. Mater. Chem. A* **2014**, *2*, 5597–5601. [[CrossRef](#)]



© 2018 by the authors. Licensee MDPI, Basel, Switzerland. This article is an open access article distributed under the terms and conditions of the Creative Commons Attribution (CC BY) license (<http://creativecommons.org/licenses/by/4.0/>).